Single View Reconstruction of Curved Surfaces

Mukta Prasad, Andrew Zisserman
University of Oxford, U.K.
http://www.robots.ox.ac.uk/~{mukta,vgg}

Andrew Fitzgibbon
Microsoft Research, Cambridge, U.K.
http://www.research.microsoft.com/~awf

Abstract

Recent advances in single-view reconstruction (SVR) have been in modelling power (curved 2.5D surfaces) and automation (automatic photo pop-up). We extend SVR along both of these directions. We increase modelling power in several ways: (i) We represent general 3D surfaces, rather than 2.5D Monge patches; (ii) We describe a closed-form method to reconstruct a smooth surface from its image apparent contour, including multilocal singularities ("kidney-bean" self-occlusions); (iii) We show how to incorporate user-specified data such as surface normals, interpolation and approximation constraints; (iv) We show how this algorithm can be adapted to deal with surfaces of arbitrary genus. We also show how the modelling process can be automated for simple object shapes and views, using a-priori object class information. We demonstrate these advances on natural images drawn from a number of object classes.

1. Introduction

The reconstruction of 3D objects from 2D images has long been of interest to researchers in computer vision and computer graphics. Our objective in this paper is to reconstruct a smooth 3D model from a single image, and in particular to compute a 3D model which projects exactly to the object outline (or *apparent contour*) in the image. This is an instance of *single-view reconstruction*: the problem of fitting 3D geometry and a camera projection to a 2D image. We follow two recent strands of research: the modelling of curved 3D surfaces [10, 15] and the automation of single-view segmentation and modelling using object class recognition techniques [6].

Horry *et al*.'s 1997 "Tour into the picture" [7] might be considered the first SVR system, allowing piecewise planar reconstructions of paintings and photographs. Subsequent systems [1, 13] improved the geometric accuracy of SVR—particularly for scenes with multiple vanishing points or planes—as well as demonstrating the extraction of (relative) metric information from uncalibrated pictures, or even renaissance paintings. However, the above systems remained essentially restricted to planar scenes. In parallel, reconstruction of special classes of curved surfaces, such as surfaces of revolution and straight homogeneous generalized cylinders [16], was developed by several authors. Utcke and Zisserman [15] give a recent survey. By specifiying the local surface normal, height, and surface discontinuities, relatively complex scenes could be extracted. However the surface representation was rather limited, being restricted to $2\frac{1}{2}$D Monge patches. Prasad *et al*. [10] extended this scheme to allow the reconstruction of 3D mesh surfaces of simple topology given simple apparent contour constraints, and providing all of the contour generator is visible.

Figure 1. Single-view reconstruction of a curved object from its apparent contour. Our method computes the global optimum of surface smoothness while exactly matching complex apparent contours arising from multilocal events.

Related to this is work on the shape from silhouette problem. The reconstruction of curved surfaces from the apparent contour was considered by Terzopoulos *et al*. [14] in their work on symmetry seeking models. In these techniques, a snake is initialized around the object outline, and image-based forces latch this snake to the projection of a parametrized 3D shape. However this and related methods were iterative, and maintaining a consistent mesh through the iterations is problematic. More recent level-set techniques [2] greatly reduce the consistency problem, but remain iterative solutions, prone to being stuck in local minima.

We focus in this paper on extending the class of linear solutions, attracted by its global optimality guarantees, and

extend the methods to deal with more complex topologies, and to deal with the case where the apparent contour displays discontinuities (see figure 1).

A second recent strand in single-view reconstruction is automation. Hoiem *et al*. [6] apply methods from the recent object recognition literature to learn texture and segmentation cues for a number of common object classes (e.g. buildings, sky, ground plane). These cues yield an approximate segmentation of the source image which can be refined by fitting a piecewise-planar 3D model to the scene, resulting in a "photo pop-up".

For curved surfaces of the type we shall consider, an important first first step in fully automating 3D pop-out is obtaining the apparent contour. Methods like GrabCut [12] can segment out an object given user supplied information about its foreground distribution (e.g. by drawing a bounding box). This is taken a step further in OBJCUT [9] where models of particular object classes (cows, horses) are learnt in advance, and no user interaction is required to segment out objects of learnt classes.

Class-specific 3D reconstruction may also be learned when a database of 3D models or multi-camera views is available. Romdhani and Vetter [11] use a linear basis for the 3D shape and then MAP estimation to instantiate shape from a single image, while Grauman *et al*. [3] learn to generate virtual views from a single silhouette from which a visual hull can be computed. Our long-term goal is to allow photo pop-up for a variety of curved shapes for which 3D models may not be readily available (glass, flowers), so we prefer to learn an object-specific 2D segmentation and to combine that with a generic 3D modelling method.

The paper outline is as follows. In section 2 we describe our closed-form solution to reconstruction from a single-view silhouette in the presence of multilocal singularities. In section 4 we show how object-recognition cues can be used to generate automatic pop-up of curved objects. We conclude in section 5 with a discussion of our results and with directions for development of this work.

2. Smooth surface reconstruction subject to apparent contour constraints

In this section we describe the basic framework for obtaining a smooth 3D object from an image. The model is obtained by minimizing a surface smoothness objective function subject to constraints from the apparent contour. We will describe the method first for a simple view of a surface with cylindrical topology (see figure 2), and then introduce the generalizations for other topologies (genus 0,1,2) and more general viewpoints.

2.1. Surface representation and generation

Following Terzopoulos *et al*. [14] we use the standard parametric surface representation, $\mathbf{r} : [0,1]^2 \mapsto \mathbb{R}^3$, since this allows us to model truly 3D freeform surfaces. The continuous surface S is denoted as $\mathbf{r}(u,v) = (x(u,v), y(u,v), z(u,v))^\top$. The surface is computed by minimizing a smoothness objective function (the *thin-plate energy* [4] or *bending energy*)

$$E(\mathbf{r}) = \int_0^1\int_0^1 \|\mathbf{r}_{uu}\|^2 + 2\|\mathbf{r}_{uv}\|^2 + \|\mathbf{r}_{vv}\|^2 \,\mathrm{d}u\,\mathrm{d}v \qquad (1)$$

subject to the constraint that the surface's contour generator projects to the given image contour. To optimize this we choose a gridded discretization (recently dubbed the *geometry image* [5]), representing $\mathbf{r}$ by three $m \times n$ matrices, $\mathtt{X}, \mathtt{Y}, \mathtt{Z}$. When solving for the surface, we shall reshape and stack these matrices into a single vector $\mathbf{g} = \left[\mathbf{x}^\top\ \mathbf{y}^\top\ \mathbf{z}^\top\right]^\top$ where lowercase $\mathbf{x}$ represents the reshaping of $\mathtt{X}$ into a column vector. Central difference approximations are used for the first and second derivatives on the surface, and are represented by appropriate matrix operators [15]. Thus the first derivative term x_u at a point (i,j) is discretely approximated as

$$\mathtt{X}_u(i,j) = \mathtt{X}(i+1,j) - \mathtt{X}(i-1,j),$$

ignoring boundary bookkeeping and scaling for the moment. This is conveniently represented by a constant $mn \times mn$ matrix $\mathtt{C}_u$ such that $\mathbf{x}_u = \mathtt{C}_u\mathbf{x}$. A similar matrix $\mathtt{C}_v$ computes the central difference with respect to v, and we term these two matrices the Jacobian operator matrices with respect to u, v. Similarly the second derivatives are computed using Hessian operator matrices denoted $\mathtt{C}_{uu}, \mathtt{C}_{uv}$ and $\mathtt{C}_{vv}$. In terms of these, then, the bending energy (1), can be expressed in discrete form as a quadratic function of $\mathbf{g}$:

$$\epsilon(\mathbf{x}) = \mathbf{x}^\top(\mathtt{C}_{uu}^\top\mathtt{C}_{uu} + 2\mathtt{C}_{uv}^\top\mathtt{C}_{uv} + \mathtt{C}_{vv}^\top\mathtt{C}_{vv})\mathbf{x} \qquad (2)$$

$$E(\mathbf{g}) = \epsilon(\mathbf{x}) + \epsilon(\mathbf{y}) + \epsilon(\mathbf{z}) \qquad (3)$$

$$= \mathbf{g}^\top\mathtt{C}\mathbf{g} \qquad (4)$$

where $\mathtt{C}$ is $3mn \times 3mn$ square matrix.

In the following subsections we introduce *linear* constraints from the apparent contour of the form $\mathtt{A}\mathbf{g} = \mathbf{b}$. This linearity is important because it leads to a standard minimization of a quadratic form $\mathbf{g}^\top\mathtt{C}\mathbf{g}$ subject to linear constraints. This problem has a unique solution which may be readily obtained using standard numerical methods.

2.2. The Apparent Contour Constraint

Terminology: The image outline of a smooth surface S results from surface points at which the imaging rays are tangent to the surface [8].

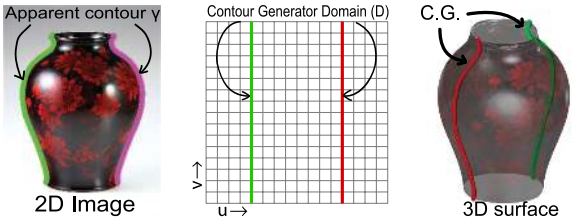

(a) (b) (c)

Figure 2. **Reconstruction of 3D surface from apparent contour constraints.** (a) The apparent contour is marked on the input image. (b) If optimizing curvature, we are at liberty to place the contour generator's domain (see §2.2) anywhere in the parameter space, providing topological constraints are maintained. In practice we minimize an approximation to curvature. A reasonably finely sampled parametrization yields good results, and allows a global optimum to be found. (c) Reconstructed surface, with contour generator superimposed. Our contribution is to extend this construction to cases where the CG is not simple.

The *contour generator* (CG) $\mathbf{\Gamma}$ is the set of points $\{\mathbf{c}\,(t) \mid 0 \leq t \leq 1\}$ on S at which rays from the viewer are tangent to the surface. The image of the contour generator is called the *apparent contour* γ, and is the set of points $\mathbf{s}$ which are the image of $\mathbf{c}$, i.e. γ is the image of $\mathbf{\Gamma}$. The apparent contour is also called the "outline", "profile", or "silhouette".

The CG is a 3D curve on the surface. If the surface is viewed in the direction of $\mathbf{r}$ from the camera centre, then the surface appears to fold, or to have a boundary or contour generator.

The apparent contour constraints can be summed up as:

- The candidate 3D model *must* project to the 2D apparent contour. We assume orthographic projection, which is adequate for the approximate models we are building.
- At the CG, the surface must also be tangent to the viewing direction.

These important image-based constraints are readily available.

The CG's *domain* is a curve in the (u, v) parameter space. If that curve is $\mathbf{D} = \{\mathbf{d}(t) = (u(t), v(t)) | 0 \leq t \leq 1\}$ then the CG is $\mathbf{c}(t) = \mathbf{r}(u(t), v(t))$. We are given an image apparent contour $\gamma = \{\mathbf{s}(t) | 0 \leq t \leq 1\}$ *i.e.* γ is the infinite set of 2D points on the apparent contour and we are assuming it is parametrized by the same t as the CG. At each point on the 2D apparent contour, we can compute the 2D unit normal (n_x, n_y). Under orthographic projection along Z, the corresponding 3D normal at the CG $\mathbf{n}$, must have a Z component of zero. Therefore, the 3D normal at t is given by $\mathbf{n}(t) = (n_x, n_y, 0)$. This means we know the surface normal at any point on the contour generator, so the (infinite) set of linear constraints which force the apparent contour of the 3D surface $\mathbf{r}$ to coincide with $\mathbf{s}$ are

$$\begin{pmatrix} 1 & 0 & 0 \\ 0 & 1 & 0 \end{pmatrix} \mathbf{r}(u(t), v(t)) = \mathbf{s}(t) \qquad \text{[Projection]} \qquad (5a)$$

$$\mathbf{n}(t)^\top \mathbf{r}_u(u(t), v(t)) = 0 \qquad \text{[Normal]} \qquad (5b)$$

$$\mathbf{n}(t)^\top \mathbf{r}_v(u(t), v(t)) = 0 \qquad \text{[Normal]} \qquad (5c)$$

Prasad *et al*. [10] observe that there is a freedom in the parametrization, so that the curve in (u, v) space which is the pre-image of the contour generator can be *chosen*. This means that $(u(t), v(t))$ in the above constraints are *known* points. For the case of a cylinder from a simple viewpoint, curves of constant u in the (u, v) are chosen as the domain of the CG—see the vertical bold lines in figure 2. In particular we choose the uniformly spaced curves $u = u_l = \frac{1}{4}, u = u_r = \frac{3}{4}$, to coincide with the CG.

In a discrete setting, each segment of the contour generator is represented by a set of 2D edgel points, the result of Canny edge detection and linking. Let us consider just the left segment, corresponding to $u = u_l$. The 2D curve is approximately arc-length sampled at n points, giving 2D points $\{(s_j, t_j)\}_{j=1}^n$, with associated 2D normals (p_j, q_j). If we let (i_l, j) in general be the integer grid coordinates corresponding to parameter space location (u_l, v), then we may write the above constraints in terms of our discretization as

$$\mathtt{X}(i_l, j) = s_j \qquad j = 1..n \qquad (6a)$$

$$\mathtt{Y}(i_l, j) = t_j \qquad j = 1..n \qquad (6b)$$

$$p_j \mathtt{X}_u(i_l, j) + q_j \mathtt{Y}_u(i_l, j) = 0 \qquad j = 1..n \qquad (6c)$$

$$p_j \mathtt{X}_v(i_l, j) + q_j \mathtt{Y}_v(i_l, j) = 0 \qquad j = 1..n \qquad (6d)$$

amounting to $4n$ linear constraints on $\mathtt{X}$ and $\mathtt{Y}$ (remembering that $\mathtt{X}_u$ is linear in $\mathtt{X}$ etc). By reshaping matrices appropriately, these may be rewritten as a matrix equation of the form $\mathtt{A}_l \mathbf{g} = \mathbf{b}_l$, where $\mathtt{A}_l$ is of size $4m \times mn$. We can repeat this process for the other contour generator segment, giving constraints $\mathtt{A}_r \mathbf{g} = \mathbf{b}_r$. Stacking these matrices, and others we shall see later, into a single large matrix yields the complete set of linear constraints $\mathtt{A}\mathbf{g} = \mathbf{b}$. The minimization of $E(\mathbf{g})$ from (4) above is then standard [15]: our objective function is quadratic and constraints are linear. This means that we can formulate a Lagrangian for the problem as

$$L = \mathbf{g}^\top \mathtt{C}\mathbf{g} + \lambda^\top (\mathtt{A}\mathbf{g} - \mathbf{b}) \qquad (7)$$

Optimizing this Lagrangian is equivalent to solving the matrix equation given by,

$$\begin{bmatrix} \mathtt{C} & \mathtt{A}^\mathtt{T} \\ \mathtt{A} & \mathtt{0} \end{bmatrix} \begin{bmatrix} \mathbf{g} \\ \lambda \end{bmatrix} = \begin{bmatrix} \mathbf{0} \\ \mathbf{b} \end{bmatrix} \qquad (8)$$

which is readily achieved using sparse methods.

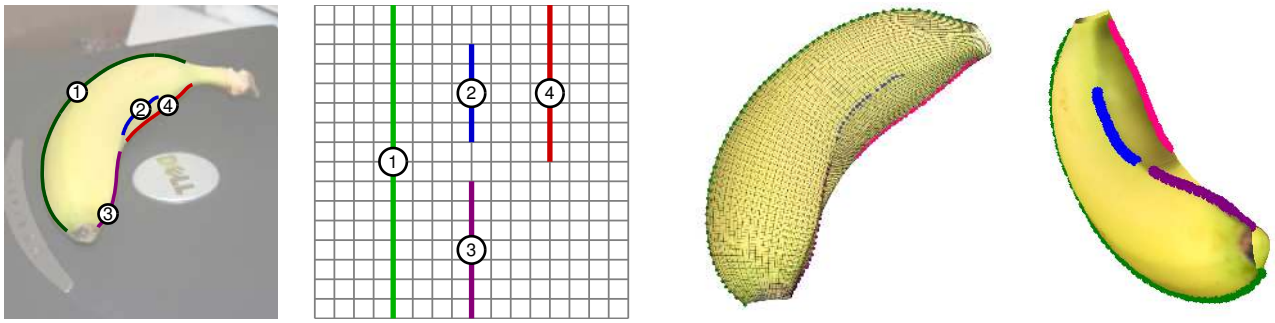

(a) (b) (c) (d)

Figure 3. **Reconstruction from a complex apparent contour.** (a) Input image, with user-selected Canny edge chains. Curve 1 is a simple segment of the apparent contour. Curves 3 and 4 represent a continuous segment of the apparent contour which corresponds to a discontinuity in the 3D contour generator. Curve 2 is a crease discontinuity which extends curve 3. (b) These curves may be laid out in parameter space so as to preserve their incidence relationships. (c,d) Projections of the recovered 3D surface from two views.

2.3. Inflation constraints

The constraints expressed in (5) constrain the x and y coordinates of the surface only. There are no constraints imposed on z. Our approximation to curvature in the form of the bending energy does not couple the z energy to that of the x and y terms, meaning that contour constraints produce a surface which projects correctly to the apparent contour but has $z(u,v) = 0\ \forall u,v$. In order to avoid this trivial solution we need to "inflate" the surface and flesh it out into a plausible model. To achieve this, depth constraints are supplied and the surface is fitted to either *interpolate* or *approximate* these constraints.

An **interpolation constraint** is of the form

$$\mathbf{r}(u_k, v_k) = \mathbf{r}_k \tag{9}$$

for given $(u_k, v_k, \mathbf{r}_k)$, the subscript indicating that there might be several such constraints. Constraints may also be supplied on just a single component of a point's position, such as its depth, $z(u_k, v_k) = z_k$. For example, we may insist that the surface passes through the plane $z = 1$ at $(u,v) = (\frac{1}{2}, \frac{1}{2})$, and the plane $z = -1$ at $(u,v) = (0, \frac{1}{2})$. Each of these constraints may again be expressed as linear functions of the surface discretization $\mathbf{g}$.

For the vase in figure 2, the inflation constraints provided were interpolation constraints which assumed the surface to be a fronto-parallel surface of revolution. Although this is a simple strategy, it still pays to use the general framework, because it guarantees that the contour generator projects correctly. If the contour generator does not project correctly (as can happen when simply constructing a surface of revolution from the image contour), texture mapping gathers pixels from the background, leading to a nasty stain on the object surface.

The reconstruction, produced by these constraints, expressed at particular parameter locations, depends on the (u,v) locations. But for simple surfaces the sensitivity to choice of (u,v) is generally low, as seen in §3.4 and figure 6. For more complex surfaces however, or where there is significant foreshortening, it is useful to supply **approximation constraints**. Approximation constraints cause the surface to pass near certain 3D points, for example, by minimizing an additional energy term of the form

$$\alpha_k \|\mathbf{r}(u_k, v_k) - \mathbf{r}_k\|^2 \tag{10}$$

The factor α_k controls the extent to which each constraint should be satisfied. A collection of such constraints may be represented as the quadratic term $\|\mathtt{M}\mathbf{g} - \mathbf{m}\|^2$ (embedded with α), giving the modified Lagrangian

$$L = \mathbf{g}^\top \mathtt{C}\mathbf{g} + \|\mathtt{M}\mathbf{g} - \mathbf{m}\|^2 + \lambda^\top (\mathtt{A}\mathbf{g} - \mathbf{b}) \tag{11}$$

Optimization of this Lagrangian boils down to the slightly modified matrix equation shown below.

$$\begin{bmatrix} \mathtt{C} + \mathtt{M}^\top\mathtt{M} & \mathtt{A}^\top \\ \mathtt{A} & \mathtt{0} \end{bmatrix} \begin{bmatrix} \mathbf{g} \\ \lambda \end{bmatrix} = \begin{bmatrix} \mathtt{M}^\top\mathbf{m} \\ \mathbf{b} \end{bmatrix} \tag{12}$$

As an example of the application of these constraints, the surface in figure 3 was constrained to approximately meet the planes $z = my \pm 1$ using the constraints $z(0.5, v) \approx mv + 1; z(1.0, v) \approx mv - 1$. The value of m is determined interactively in order to obtain the best-looking shape.

3. More General Surfaces and Views

In this section we increase the scope of single-view reconstruction in two ways: first, we deal with more complicated viewpoints. These are still generic viewpoints, but now the apparent contour may terminate (where the view direction is asymptotic) or be self occluded (a bi-local event); second we generalize the topology, and move from cylinders to spheres, and from genus zero to genus 1 and 2.

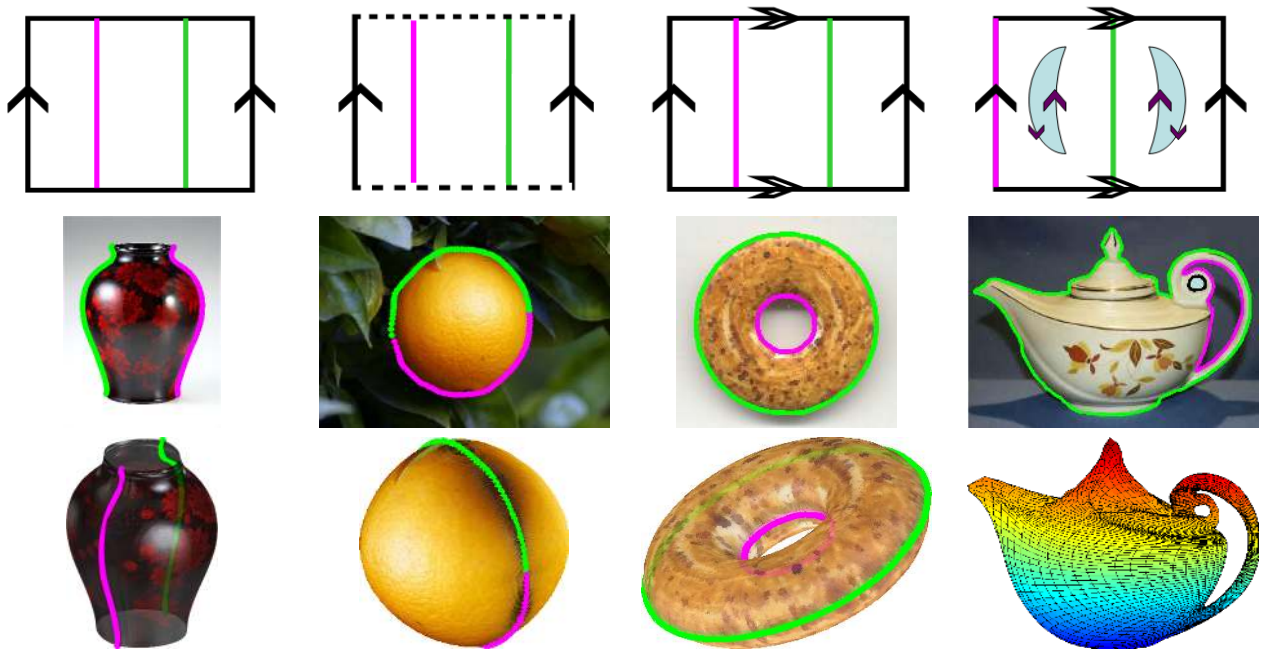

(a) Genus 0 (cylindrical) (b) Genus 0 (spherical) (c) Genus 1 (toroidal) (d) Genus 2 parametrization

Figure 4. **Topology**. The first row shows the parameter space for each of the topologies listed in the bottom row. The arrow types indicate which ends of the parameter space must join with each other. The dotted line in column 2 indicates that all points on that parameter line join at one point. For surfaces of genus > 1, the hole in the surface translates to two holes in the parameter space as shown in column 4. Images and reconstructions of surfaces of the respective topologies are shown on Rows 2 and 3, with the apparent contour constraint represented as green and magenta curves.The genus 2 teapot without texture mapping demonstrates the power of the parametrization

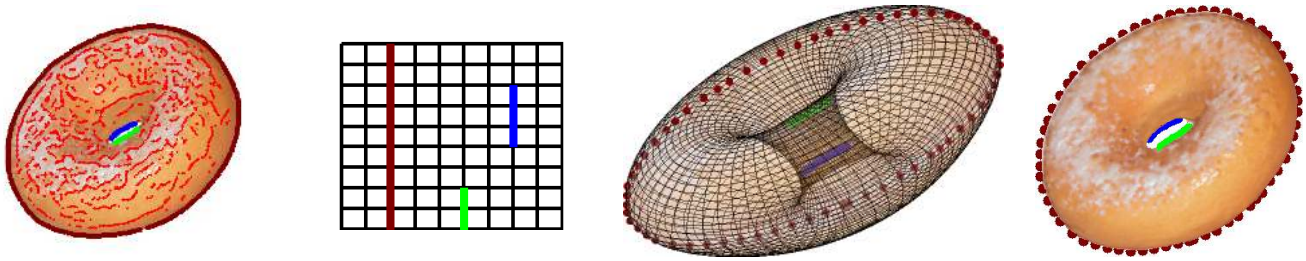

(a) (b) (c) (d)

Figure 5. **Discontinous contour generator, torus topology.** (a) Donut image, with Canny edgels superimposed. The three segments of the contour generator are shown thickened. (b) Contour generator segments in parameter space. (c) Inflated surface, contour generator visible through transparency. (d) Textured model.

3.1. Discontinuous contour generators

In case of objects which are self-occluding, the entire object's contour generator cannot be identified with a constant u curve in the parameter space. Continuous parts of the apparent contour which project from locally continuous regions of the object are identified from their image projections (see the coloured curves in figure 3). The ordering and relative scale and position of these curve segments on the surface is associated approximately with their locations on the parameter space. Again we use the freedom in the (u, v) parametrization to choose these as parts of constant u or constant v curves in the parameter space. The position of the constraint curves on the parameter space is flexible, up to ordering, and if scale and position in the mapping of these curve segments are preserved roughly, the reconstruction will adhere well to the apparent contour constraints. Given the parameter-space cuts, a number of new constraints are introduced into the system of equations.

We refer now to the banana image in figure 3, whose caption should be perused before continuing. The four curves introduce new constraints of the type outlined above. The

left-hand side of the apparent contour is handled just as above (6) (note that in this example the CG is non-planar—this is handled perfectly using the previous machinery). Curves 4 and 3 are simply segments of contour generator handled as above, noting that they must not occupy the same u = constant curve in parameter space because they are disjoint on the object. Denote curve 3 as extending from $(u_3, 0)$ to (u_3, v_3), and curve 4 from (u_4, v_4) to $(u_4, 1)$. It is not important where the curve endpoints are placed in the v direction, although it uses grid resolution most effectively if they are placed so that the curves are roughly arc-length parametrized when re-projected into the image.

Curve 2 is a particular class of curve on a 3D object. Because it corresponds to a crease discontinuity, it is visible in the image after it has ceased to be part of the contour generator. Thus we can identify it, and assign it to the same u-constant parameter line as curve 3. This creates a more pleasing parametrization and generates a more plausible 3D model, in conjunction with crease discontinuity handling (§3.3).

3.2. Topology

The parametric surface representation allows us to represent surfaces of different topology and shape. As with the contour generator, topology can be represented quite readily by various cuttings of the parameter space. Although somewhat complex, these cuttings need be worked out only once per topological class. Figure 4 illustrates the various cases, and we consider some examples to show how these are implemented in our optimization framework.

For the **cylindrical** topology of figure 4, the essential constraint is that points on the $u = 0$ curve (i.e. the 3D curve $\{\mathbf{r}(0, v) | 0 \leq v \leq 1\}$) are neighbours of points on the $u = 1$ curve. In a continuous parametrization, it would be natural to implement this as a set of incidence constraints on the surface and its derivatives

$$\mathbf{r}(0, v) = \mathbf{r}(1, v) \quad \forall v, \tag{13a}$$

$$\mathbf{r}_u(0, v) = \mathbf{r}_u(1, v) \quad \forall v, \tag{13b}$$

$$\mathbf{r}_{uu}(0, v) = \mathbf{r}_{uu}(1, v) \quad \forall v, etc. \tag{13c}$$

which is again linear in $\mathbf{r}$. In a discrete implementation, this is a waste of $1/m$ of the parameter space and complicates bookkeeping. In practice it is simpler to make $\mathtt{X}(1, j)$ and $\mathtt{X}(m, j)$ neighbours in the derivative computations by modifying the Jacobian operator matrix $\mathtt{C}_u$, as well as the appropriate second derivative operators. For **spherical** topology, these incidence constraints are augmented with the constraints that: (i) $\mathbf{r}(u, 0) = \mathbf{r}(0, 0) \forall u$ which is again linear in $\mathbf{r}$, and is implemented as the $3m$ linear constraints; and (ii) $\mathbf{r}_v(u, v) = r_v \left(\left(u + \frac{1}{2} \right) \bmod 1, v \right) \forall u; v \in \{0, 1\}$. The **torus** topology is a straightforward modification of the cylindrical case. Finally, higher genus surfaces require somewhat more profligate use of the parameter space. To make a genus two surface requires that two loops of parameter space are identified. In this case, modification of the derivative operator matrices is not for the faint-hearted, and recourse to a simple parameter identification as in (13) is probably the best course of action. One such implementation of a genus 2 surface can be seen in figure 4. For a logical choice of the loop and a reasonable resolution, the precise choice does not greatly affect surface shape.

3.3. Surface creases

One final generalization is to allow the surface to crease. This means, as with the apparent contour, specifying a curve in the parameter space (say $u = u_c$), and constraining points along this curve to project to the image of the crease as in (5a). The second modification is to $E(\mathbf{r})$: replacing the bending energy, computed from second derivatives, with a membrane energy—the sum of squares of first derivatives across the curve. Considering the contribution to $E(\mathbf{r})$ at a point (u_c, v) on the crease, we replace

$$\|\mathbf{r}_{uu}\|^2 + \|\mathbf{r}_{uv}\|^2 + \|\mathbf{r}_{vv}\|^2$$

with

$$\|\mathbf{r}_{uu}\|^2 + \|\mathbf{r}_v\|^2$$

so that the term transverse to the curve permits high second derivatives, allowing the crease to form when E is minimized. This is implemented by augmenting $\mathtt{C}$ with first-derivative terms, and adding weights to control the influence of each row of $\mathtt{C}$. The energy remains quadratic in the surface $\mathbf{g}$ and a global minimum is easily found.

3.4. Sensitivity to parameter assignment

At several points throughout the paper we make special choices of parameter-space points and curves, remarking that the precise values chosen will have a minimal effect on the recovered surface. In theory this is true if the energy being minimized is invariant to parametrization, for example surface curvature. In practice we are not minimizing curvature, merely a proxy for it. This proxy computes derivatives in the parametric space and does not take actual 3D distances into account. So the parametrization does affect the object shape. We illustrate that this effect is small by perturbing our assignments in the parameter space by approximately 20% of their original assignment values for the banana example. The models produced using identical inflation are shown in figure 6. Varying the parameter assignment results in different but all convincing models. The sensitivity to perturbation also depends on the object complexity and the availability of constraints. One workaround is to use derivatives weighted by 3D distances and find the optimal surface by iteratively fitting and reparametrizing the surface.

The object shape is closely related to the density of parametrization. For an object with large variations in curvature, parametrizing sufficiently densely that the high-curvature sections are modelled will waste effort in densely sampling near-planar areas. These questions are among those addressed by Gu *et al*.'s "geometry image" work [5].

4. Automation

Complete automation of single view reconstruction for particular curved surface classes requires a number of steps: (i) Detect the apparent contour curves—for example by segmenting out the object; (ii) identify the contours in the parameter space; (iii) generate a surface consistent with apparent contours (this may require inflation hints); (iv) texture map the surface from its image appearance. We have demonstrated steps (iii) and (iv), we now address step (i): segmenting out the object automatically.

For segmentation we employ the OBJCUT formulation of Kumar *et al*. [9]. In this method, segmentation is treated as a binary MRF labelling problem. The MRF includes likelihoods from the foreground and background colour/texture distributions, and the segmentation is guided by a pictorial structure object model (the pictorial structure prior is what OBJCUT adds to the model over earlier work such as GrabCut [12]). The initial distributions and pictorial structure are learnt from training images of the object class.

In brief, we use 25 training images for oranges and 30 for bananas. The implementation of OBJCUT is from code supplied by the authors of [9]. This algorithm is successful in segmenting many of the images. There are occasional problems when the initial chamfer match of the pictorial structure is attracted to erroneous edges.

Figure 7 shows examples of completely automated reconstructions. These involve segmentation (with OBJCUT) and the assumption that the views are simple for each class (so that the apparent contour may be identified with the segmentation boundary). Of course, in the case of an orange, there are only simple views.

5. Discussion

We have presented several new extensions of recent work on modelling smooth shapes from their apparent contours. In particular we have demonstrated the accurate recovery of a 3D parametric surface with a discontinuous, non-planar contour generator. Our method results in a system of linear equations, yielding the globally optimal energy. In addition, we have shown how the modelling framework can be extended to deal with complex topologies, again with discontinuous contour generators.

The issues discussed in §3.4 must be dealt with. To avoid the challenges posed by non-linear minimization methods, we hope to solve these problems with a more realistic energy and iterative minimization methods.

Finally, the inflation strategy we use is also a by-product of not minimizing curvature. It is somewhat clumsy and increases the amount of user skill required to make models. We hope to find ways of better approximating a curvature-like energy or alternatively, devise a better inflation mechanism to alleviate this difficulty.

References

[1] A. Criminisi, I. Reid, and A. Zisserman. Single view metrology. *IJCV*, 40(2):123–148, Nov 2000.

[2] O. D. Faugeras and R. Keriven. Complete dense stereovision using level set methods. In *Proc. ECCV*, pages 379–393, 1998.

[3] K. Grauman, G. Shakhnarovich, and T. Darrell. Virtual visual hulls: Example-based 3D shape inference from a single silhouette. In *Proc. 2nd Workshop on Statistical Methods in Video Processing*, 2004.

[4] W. E. L. Grimson. *From Images to Surfaces: A Computational Study of the Human Early Visual System*. MIT Press, 1981.

[5] X. Gu, S. J. Gortler, and H. Hoppe. Geometry images. In *ACM Trans. Graph.*, pages 355–361, New York, NY, USA, 2002. ACM Press.

[6] D. Hoiem, A. A. Efros, and M. Hebert. Automatic photo pop-up. *ACM Trans. Graph.*, 24(3):577–584, 2005.

[7] Y. Horry, K. Anjyo, and K. Arai. Tour into the picture: Using a spidery mesh interface to make animation from a single image. In *Proc. ACM SIGGRAPH*, pages 225–232, 1997.

[8] J. Koenderink. *Solid Shape*. MIT Press, 1990.

[9] M. Kumar, P. Torr, and A. Zisserman. OBJ CUT. In *Proc. CVPR*, pages I: 18–25, 2005.

[10] M. Prasad, A. W. Fitzgibbon, and A. Zisserman. Fast and controllable 3D modelling from silhouette. In *Eurographics, Short Papers*, 2005.

[11] S. Romdhani and T. Vetter. Estimating 3D shape and texture using pixel intensity, edges, specular highlights, texture constraints and a prior. In *Proc. CVPR*, pages II: 986–993, 2005.

[12] C. Rother, V. Kolmogorov, and A. Blake. "GrabCut": interactive foreground extraction using iterated graph cuts. *ACM Trans. Graph.*, 23(3):309–314, 2004.

[13] P. Sturm and S. J. Maybank. A method for interactive 3D reconstruction of piecewise planar objects from single images. In *Proc. BMVC.*, 1999.

[14] D. Terzopoulos, A. Witkin, and M. Kass. Symmetry-seeking models for 3D object reconstruction. *Proc. ICCV*, pages 269–276, 1987.

[15] L. Zhang, G. Dugas-Phocion, J. Samson, and S. Seitz. Single view modeling of free-form scenes. In *Proc. CVPR*, pages I:990–997, 2001.

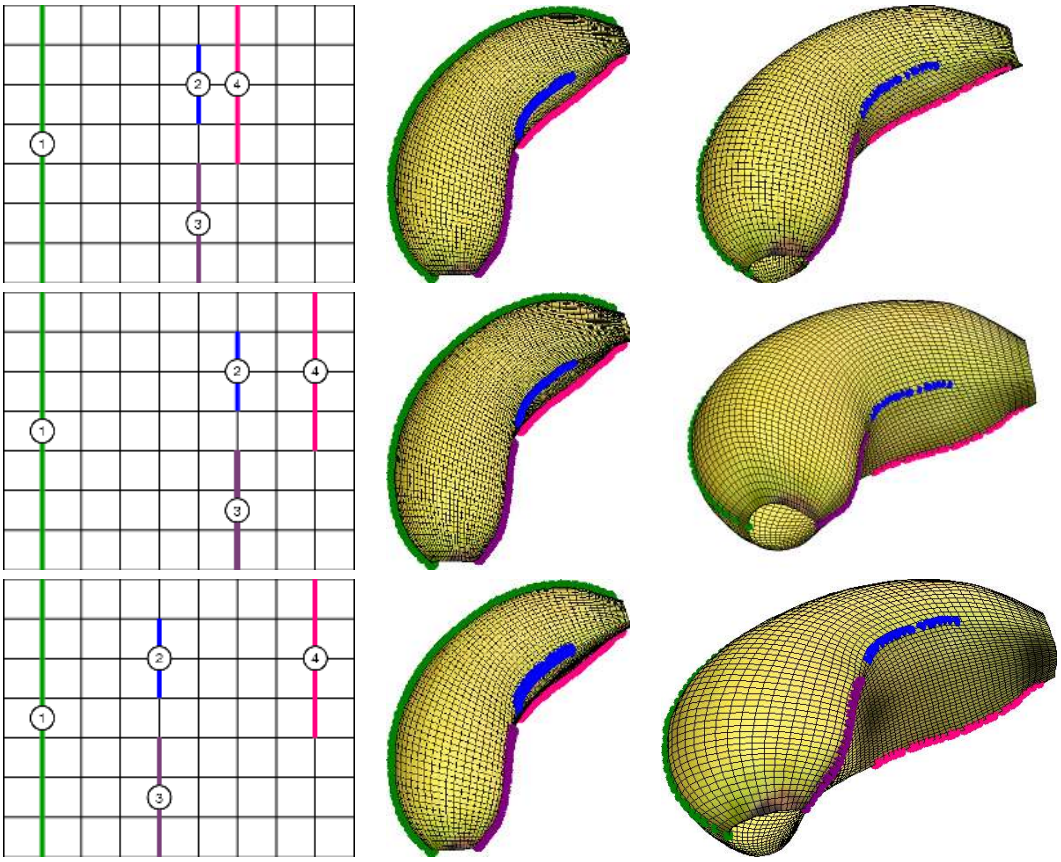

Figure 6. **Perturbing the parameter space assignment:** Column (i) shows the parameter assignment for each case. Columns (ii) & (iii) show the front and oblique views of the model respectively.

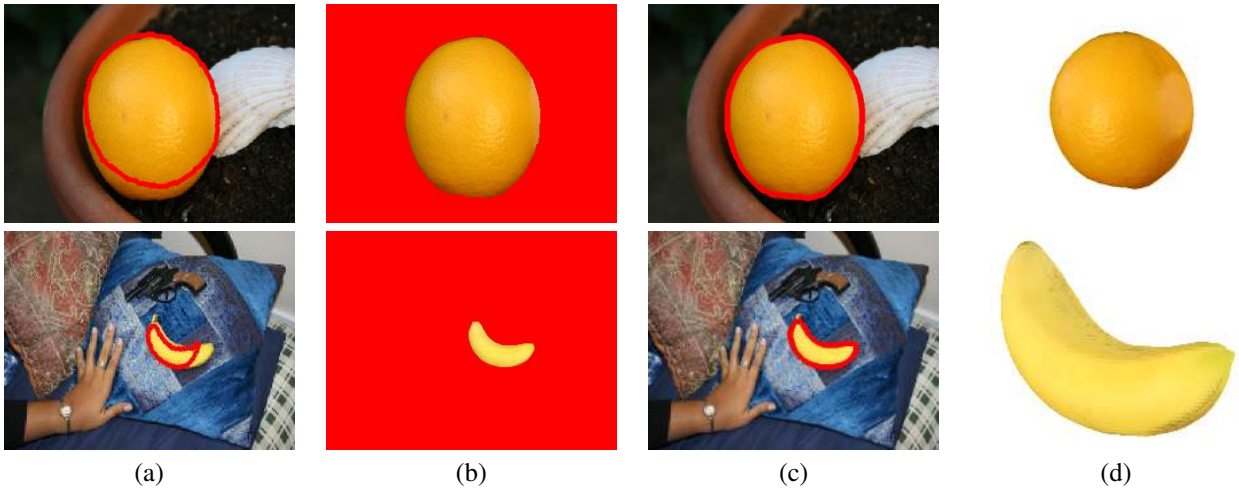

Figure 7. **Automatic reconstruction of simple objects.** (a) Two images and the best chamfer match found from the orange and banana models. (b) OBJCUT segmentaion yields a much better segmentation than the initial chamfer. (c) Contour input to the reconstruction algorithm. (d) 3D reconstruction.